Smart Structures and Systems, *Vol. 24, No. 2 (2019) 193-207*
DOI: https://doi.org/10.12989/sss.2019.24.2.193

Shape morphing and adjustment of pantographic morphing aerofoil section structure

Najmadeen M. Saeed*[1] and Alan S.K. Kwan[2a]

[1]*Department of Civil Engineering, University of Raparin, Rania, Kurdistan Region, Iraq*
[2]*Cardiff School of Engineering, Cardiff University, Cardiff CF24 3AA, U.K.*

(Received July 15, 2017, Revised February 4, 2019, Accepted May 31, 2019)

Abstract. This study concerns with morphing structures, *e.g.* as applied in the aerospace industry. A morphing aerofoil structure capable of variable geometry was developed, which was shown to be able to cater for the different aerodynamic requirements at different stages of flight. In this work, the useful and relatively simple method has been applied, which provides a direct method for calculating required morphing shape displacements via finding the most effective bar through calculating bar sensitivity to displacement and calculating set of length actuations for bar assembly to control/adjust shape imperfection of prestressable structural assemblies including complex elements ("macro-elements", e.g., the pantographic element), involving Matrix Condensation. The technique has been verified by experiments on the physical model of an aerofoil shaped morphing pantographic structure. Overall, experimental results agree well with theoretical prediction. Furthermore, the technique of multi-iteration adjustment was presented that effective in eliminating errors that occur in the practical adjustment process itself. It has been demonstrated by the experiments on the physical model of pantographic morphing structure. Finally, the study discusses identification of the most effective bars with the objective of minimal number of actuators or minimum actuation.

Keywords: morphing aerofoil; shape control; shape morphing; pantographic structure; matrix condensation.

1. Introduction

In the past few decades, interest in morphing structures has increased due to the greater benefits they can provide in numerous engineering applications, particularly within aerospace research as arranging and controlling systems, because of their variable geometry, low weight and reduced overall complexity of structure (Lachenal *et al.* 2012). A morphing structure is a structure capable of modifying its geometric characteristics and dimensions or tune its properties in order to its operating conditions, change its interaction with the surrounding environment adaptation to different load conditions (Iannucci and Fontanazza 2008). Morphing structures increased the ability of engineers to improve wing design. The basis of inspiration of morphing structures is the natural world; e.g., a bird's wing can take several different shapes for different flight requirements (Saeed and Kwan 2014). Bliss and Bart-Smith (2005) pointed out the feasibility for the morphing wing to be used for flight control. A morphing aerofoil technique by using complex composite cellular structures was investigated by Bettini *et al.* (2010). Du and Ang (2012) found that morphing aerofoil could replace the traditional hinged control aerofoil to control flight attitude with smaller drag and increased flight efficiency.

The basic composition of morphing aerofoil in this paper is morphing structure, so reviewing of the shape morphing of structures has become necessary. In the last decade an increasing variety of attractive structures and buildings with movable functions have been seen worldwide, for instance in bridges that open to allow ships to pass, revolving restaurants on tops of buildings, sliding roofs of baseball and soccer dome stadiums, and artistic monuments (Inoue 2007). Later, (Inoue 2007) progressed the movable structures that includes change in the behaviour of the structures simultaneously with the changing the geometric shape of the structures with a lively motion. Inoue presented the first application of an adaptive structure using a variable geometry truss mechanism at the International Expo 2005 in Aichi, Japan.

Since some space structures are very sensitive, they could be distorted under loading or deployed in harsh environments, it is necessary to restore or adjust such structures to the design/desired shape. This can be done by actuation of certain parameters, *e.g.* altering the length of a member (Saeed and Kwan 2014, Saeed 2014). Work on the associated analytical/computational techniques is not extensive, and this is especially the case for direct approaches. Haftka and Adelman (1985a) studied shape control by thermal effects, and via placement of actuators (Haftka and Adelman 1985b) with heuristic search. Such indirect approaches have also been tested with an algorithm of successive correction based on heuristics (Subramanian and Mohan 1996). On the other hand, You (1997) dealt with the problem directly, and showed the direct link between length actuations and displacements for prestressed structures.

*Corresponding author, Ph.D.
E-mail: Najmadeen_qasre@uor.edu.kr
[a] Professor
E-mail: Kwan@cardiff.ac.uk

http://www.techno-press.com/journals/sss&subpage=7
ISSN: 1738-1584 (Print), 1738-1991 (Online)

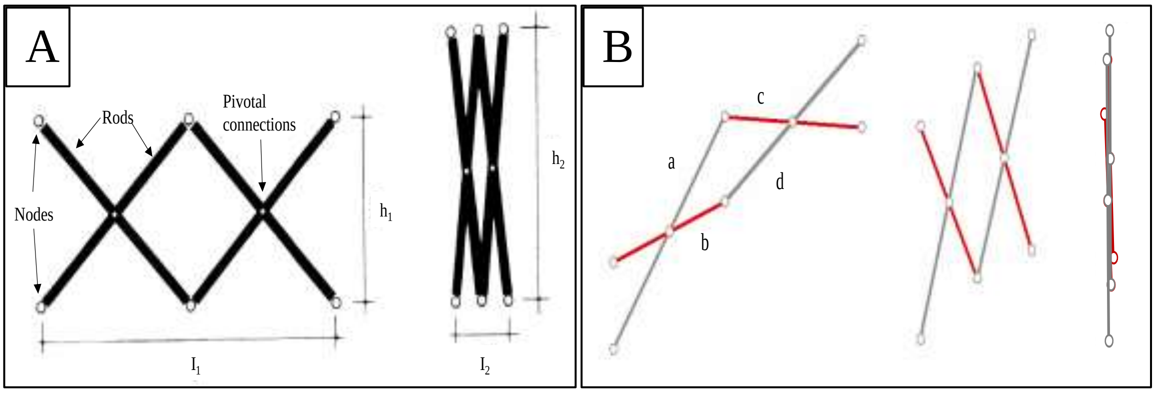

Fig. 1 The concept of a pantograph (A) and the deployability constraint in terms of the semi-lengths (B)

The purpose of this paper is theoretical and experimental calculating of the required morphing shape displacements of the physical model of pantographic morphing structure. Consequently, to show the concept for a morphing aerofoil by pantographic morphing structure is an effective way to enhance/replace the traditional aerofoil via finding the most effective bar through calculating bar sensitivity to displacement. Moreover, providing a direct relationship between bar length actuations and the nodal position/displacements for adjusting shape imperfection of the desired aerofoil theoretically and experimentally on the physical model of pantographic morphing structure made up of more complicated structural components through using the condensed matrix method. Finally, finding where the actuator should be placed indicated to lead to minimal amount of actuation and that it is possible to choose a just sufficient number of actuators.

The outline of this paper is as follows: A short review on pantographic structures will be discussed in Section 2. Concepts for morphing aerofoil sections using pantographic structures will be presented in Section 3. The technique of morphing shape calculation and finding a set of length actuation to achieve shape adjustments via Force Method through using Matrix Condensation method are illustrated in Section 4. The experimental model of morphing shape calculation and comparison of results will be shown in Section 5. Section 6 transacts finding a set of length actuation to achieve shape adjustments of the physical model of pantographic morphing structure and highlighting the most effective member in order to find minimal amount of actuation and minimal number of actuators. Finally, a concluding summary will be presented in Section 7.

2. Pantographic structures

The basic composition of morphing structures in this paper are pantographs (Pinero 1961, Gantes 2001). Pantographs are a specific type of deployable structures that are capable to deploy from a small compact state to a larger expanded state while carrying loads (Merchan 1987, De Temmerman 2007). Through rotating the rods about the pin, the structure can be elongated or flattened in the plane of the rods to change shape (Wolfe 2013) as shown in Fig. 1. Rapid deployability with minimum labour is the main advantage of pantographic structures (Chikahiro *et al.* 2014, Wolfe 2013).

Different types of basic unit types for the pantographic structure can be produced through changing the location of the intermediate hinge or the shape of the bars such as translational (Fig. 1), polar and angulated units (Hoberman 1990, You and Pellegrino 1997, Jensen and Pellegrino 2005, De Temmerman 2007, Alegria Mira 2010, Maden *et al.* 2011, Roovers and De Temmerman 2014). Akgün (2010) developed a new type of pantographic unit, called the modified pantographic unit. The introduction of kinematic degree of freedom ensures mobility and transformation of the deployment of a structure. Crucial to the design of deployable morphing structures is the “deployability constraint” which is a simple formula derived by Escrig (1985), for instance for the linkage in Fig. 1, as: ($a + b = c + d$). This equation means that for the system to fully close the sum of the semi-lengths *a* and *b* of a pantographic unit has to equal the sum of the semi-lengths *c* and *d* of the adjoining units.

3. Concepts for morphing aerofoil sections using pantographic structures

Aerofoil is a two dimensional cross-section shape of a wing, which is used to either generate lift or minimize drag when exposed to a moving fluid (Bliss and Bart-Smith 2005) with the different terminologies (Saeed and Kwan 2014). In the authors’ work (Saeed and Kwan 2014), the standard NACA2415 aerofoil was chosen as a comparator as shown in Fig. 2. This aerofoil is commonly used in light aircraft, and is part of the Four-Digit Series, which is a class of standard NACA *(National Advisory Committee for Aeronautics)* aerofoils.

3.1 Structure of proposed aerofoils

The proposed shapes of morphing aerofoil are achieved via a series of interconnected, curved, single-control pantographs. Aerofoil NACA2415 has been chosen as the base-shape for constructing both proposed shapes. Configurations of the two morphing structures one (MAS1)

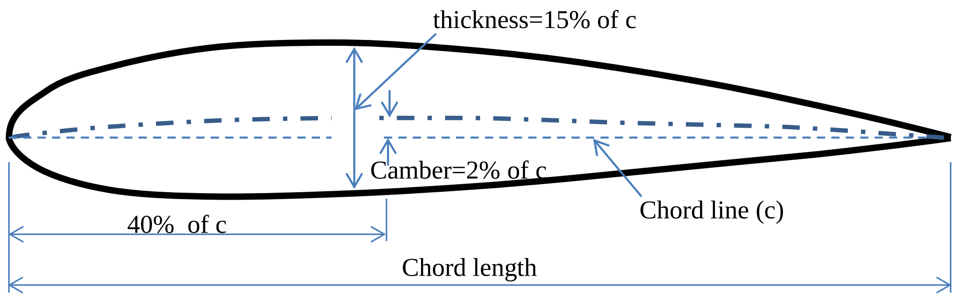

Fig. 2 Parameters of the NACA2415 aerofoil

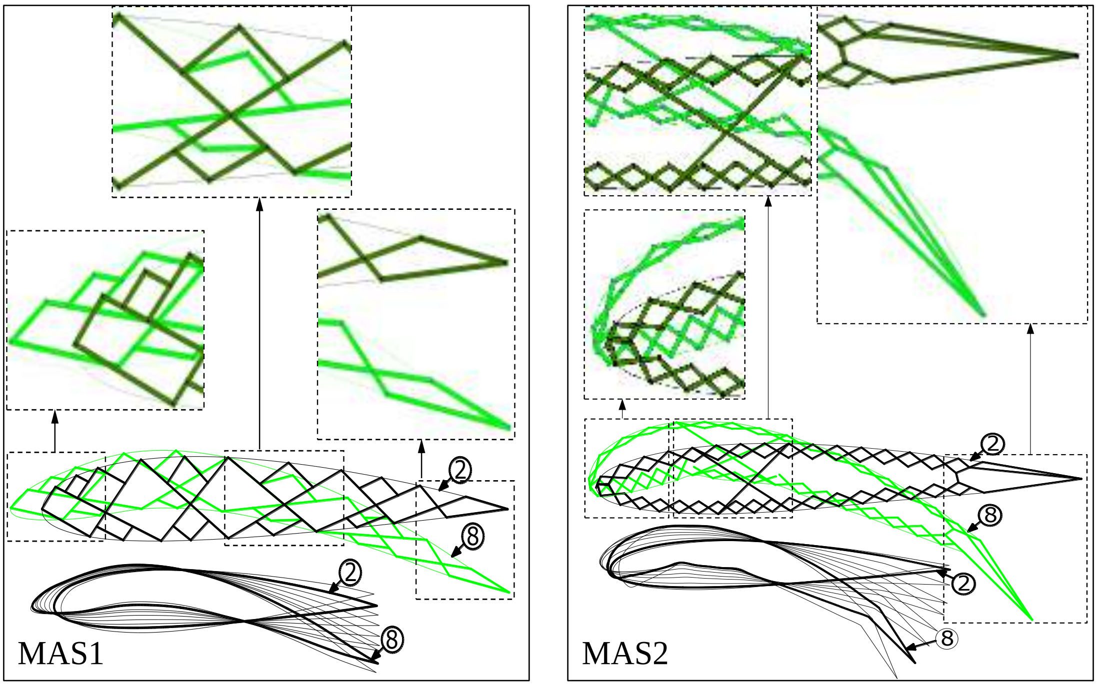

Fig. 3 Nine morphing stages of MAS1 and MAS2

and two (MAS2) are shown in Fig, 3 (Saeed and Kwan 2014). Each morphing structure also has a "control bar" (as bar 36 in Figs. 5 and 13) which is a bar of variable length that is used for controlling the shape configuration of the morphing aerofoil structure. The overall morphing pantograph mechanism has only one degree of freedom, so this control bar can be positioned in many different places, but only one is needed. In the experimental models length actuation has been effected by a turnbuckle built into the control bar.

3.2 Results of comparing C_L, C_D of the proposed aerofoils with NACA2415

For understanding the benefit of the proposed morphing aerofoil structures, it should be calculated and compared with the standard traditional hinged surface control aerofoil. The changing sectional shapes cover leading edge, chamber, thickness, width and leading edge of aerofoil to suit different flight environments (Saeed and Kwan 2014). C_L and C_D relationship of MAS1, MAS2 and standard NACA2415 are shown in Fig. 4. These coefficients are calculated from the shape of the nine morphing stages of MAS1 and MAS2 and by changing the angle of attack (fixing flap angle) and via increasing flap angles (with angle of attack remaining fixed). The figure shows that in general both MAS1 and MAS2 provide less C_D as compared to NACA2415. In addition, both the maximum C_L of MAS1 and MAS2 are greater than the peak C_L achievable by NACA2415 (Saeed and Kwan 2014). In summary, it is found that the morphing aerofoil is more effective than NACA2415 for producing bigger C_L for the same amount of C_D (Saeed and Kwan 2014).

4. Pantographic morphing structure

A model of the morphing aerofoil structure was constructed for experimental purposes. This model follows the geometry and configuration of the morphing aerofoil

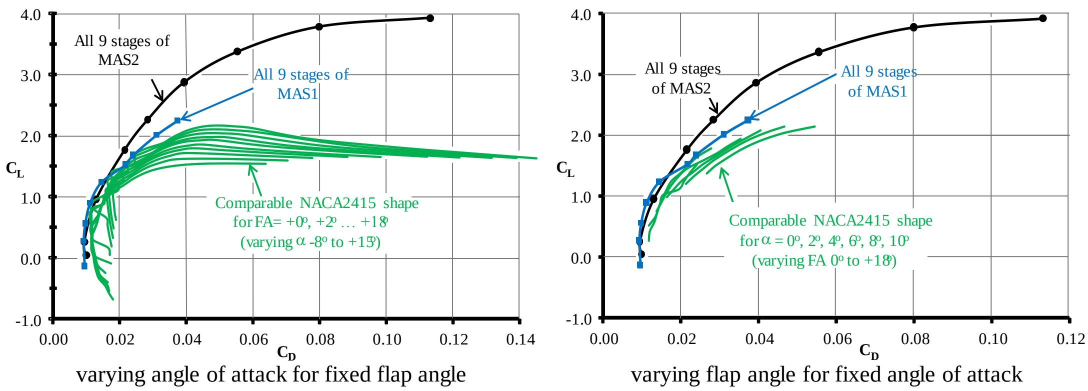

Fig. 4 Comparing C_L and C_D of NACA2415 with MAS1 and MAS2

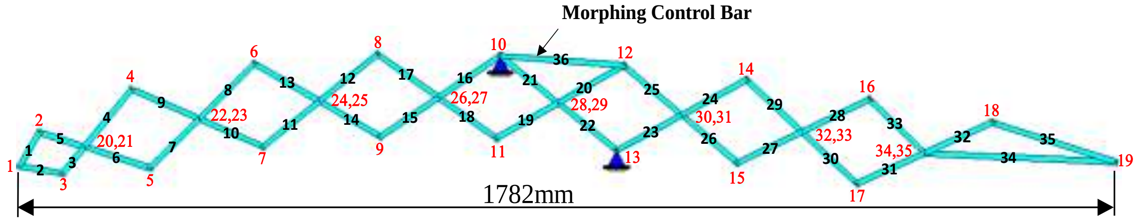

Members	Length (mm)	Members	Length (mm)	Members	Length (mm)
1	58.4	13	118.8	25	119.3
2	70.1	14	111.8	26	114.2
3	52.6	15	110.7	27	113.9
4	113.7	16	117.1	28	119.8
5	76	17	117.8	29	117.3
6	111.7	18	111.5	30	117.8
7	107.1	19	112.5	31	118.3
8	120.6	20	119.3	32	118.9
9	118.3	21	116.1	33	119.4
10	111.3	22	117.5	34	310.4
11	113.1	23	117.6	35	208.1
12	116.7	24	117	36	200.5

All Members		
Height	9.0	mm
Width	6.0	mm
EA	3,780	kN
EI	25,515	$kN.mm^2$

Fig. 5 Pantographic morphing structure model (Demonstration morphing of Aerofoil)

cross-section, as an application of the pantographic morphing structure. The model is built via series of interconnected, irregular, single-control pantographs as shown in Fig. 5. Each pantograph unit consists of two coplanar beam elements of different lengths connected together by a shear connector (scissor-like hinge) with axis perpendicular to the plane of the beams. Two adjacent pantograph-units are connected by a further shear connector at the ends of the coplanar beams. A model was constructed for the purpose of morphing and adjustment experiment of the external joint displacement. There was no adjustment of internal bar forces in any of experiments done in this paper mainly because the beams of the model are comparatively thick and thus able to sustain big axial forces, but also because the principal control of interest in the aerofoil is getting the right shape accurately, in order to obtain the desired aerodynamic characteristics. The morphing in the structure is activated through length change in the bar designated "bar 36" as shown in Fig. 5,

The technique of displacement and force control of complex element structures by matrix condensation Eq. (1) (Saeed and Kwan 2016) is applied to calculate the required morphing shape displacements and to control/adjust shape imperfection of the desired aerofoil model. Using reduced matrices of equilibrium, compatibility and flexibility, since this model is constructed from interconnecting a series of pantographic units.

$$\mathbf{d}_c = \mathbf{d}_{pc} + \mathbf{Y}_c \, \mathbf{e}_{oc} \tag{1}$$

where $\mathbf{d}_{pc} = [\mathbf{C}_1 \; \mathbf{Q}_1]^T \mathbf{t}_{nH}$ is the vector of nodal displacements of the structure due only to non-vanishing load component, $\mathbf{Y}_c = \begin{bmatrix} \mathbf{Y}_n & \mathbf{Y}_p \end{bmatrix}$, $\mathbf{Y}_n = [\mathbf{C}_2 \; \mathbf{Q}_2]^T$, $\mathbf{Y}_p = [\mathbf{C}_3 \; \mathbf{Q}_3]^T$, $\mathbf{e}_{oc} = [\mathbf{e}_{no} \; \mathbf{e}_{po}]^T$ and $\mathbf{d}_c$ is the resultant nodal displacements after some elongation actuation $\mathbf{e}_{oc}$ has been applied in the condensed matrix method. The

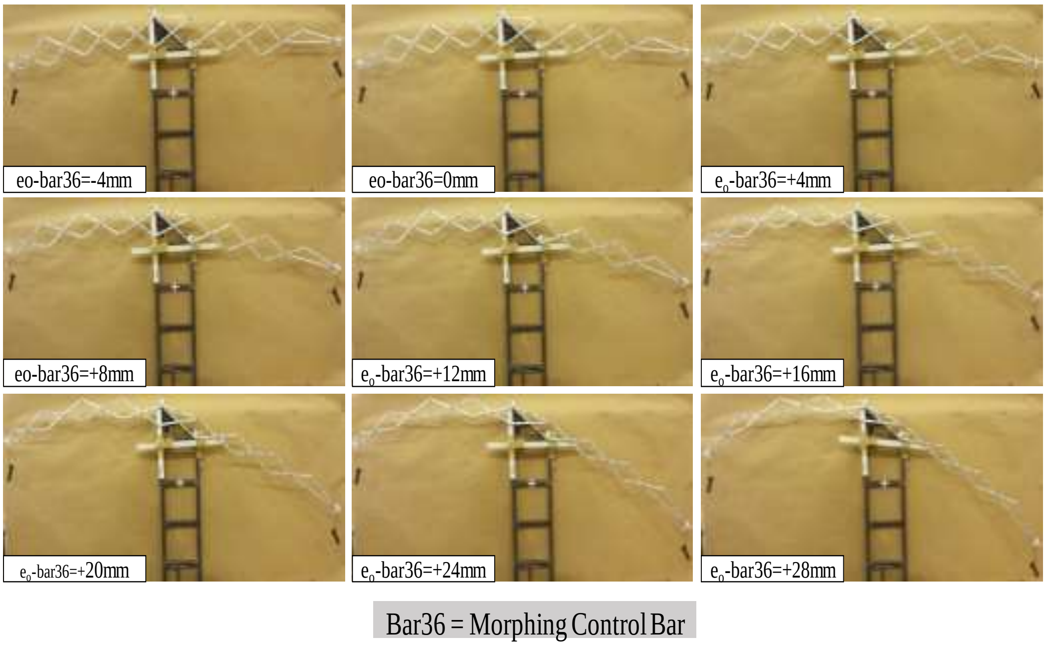

Fig. 6 Nine morphing stages of morphing structure in Fig. 5

derivation of the technique is derived in detail by Saeed and Kwan (2016).

This technique can be applied to the pantographic morphing structure model in Fig. 5 with few points and observation. The complete global equilibrium matrix (**A**) of the given model is of size 105×108, since this model consists of 36 beams and 35 joints. In order to condense the equilibrium matrix some steps must be done. Firstly, by removing four rows relating to four constraints of the two supports (*i.e.* dx_{10}, dy_{10}, dx_{13} and dy_{13}), the size of the **A** matrix becomes 101×108. Secondly, since there is no external couple applied to the internal joints, the bending moment there will be continuous in each beam-pair of the pantograph unit, the moment of both beams of a beam-pair can be replaced by a single variable. In the given model there were seven pantograph units with two half pantograph beams 31 and 32, see in Fig. 5, thus 30 mid-joint moments of all beams of pantographs can be replaced by 15 new variables, hence the size of **A** becomes 101×93. Thirdly, since the pantograph units are connected to each other at their remote ends by pin-joints, then the internal bending moment of each beam-pair at these ends are always equal to zero, and consequently all the 42 columns corresponding to these moments can be removed and the size of the **A** matrix is reduced to 101×51. Fourthly, since no external couples are applied to the mid- and end-joints of the pantograph units of the given example, the corresponding 35 rows are removed so the size of the **A** matrix reduced to 66×51.

Lastly, as there is no external load applied to the internal joints of the pantograph unit, which is just a shear-connector between two beam-pairs, the two horizontal component of load at both mid joints can be replaced by one new horizontal component, which is equal to the sum of both horizontal components. Similarly, the same can also be done for the vertical components. The given model has 16 mid joints as shown in Fig. 5, thus all 32 components of the mid-joints of the model can be replaced by 16 new components, hence the size of **A** becomes 50×51. Now the equilibrium matrix can be condensed to $\mathbf{A}^*$ by using $\mathbf{A}^* = \mathbf{A}_{mn} - \mathbf{A}_{mp}\mathbf{A}_{pp}^{-1}\mathbf{A}_{pn}$ to a size of 35×36 (Saeed 2014).

Similarly, the condensed compatibility and flexibility matrix must be calculated using the same process. Since compatibility matrix is the transpose of equilibrium matrix, the global size of **B** is 108×105, and after condensation the size $\mathbf{B}^*$ reduces to 36×35. While the global flexibility matrix starts with size 108×108, is reduced to 51×51, and after completion of condensation process, $\mathbf{F}^*$ has a size of 36×36.

5. Comparison of experimental and theoretical morphing deflection

5.1 Experimental structure morphing

Morphing requires structure to possess some form of mechanisms for mobility, for instance convenient arrangement of hinges and bars to allow shape re-configuration. In any structure the process of morphing will not work without an external source of energy or actuation of members, which is done via actuators embedded to the members of the structure.

A pantographic morphing structure in Fig. 5 was prepared for the purpose of morphing as well as for adjustment/controlling. In the morphing mechanism the structure changes significantly from one shape another, with the same number of hinges and bars, that is a large

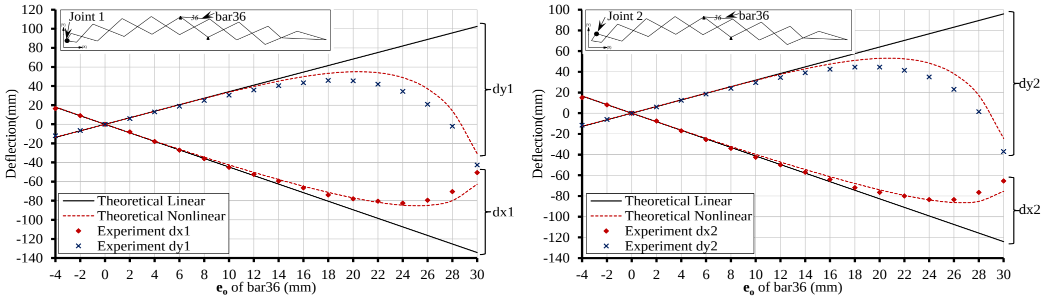

Fig. 7 Theoretical and experimental deflection of joints 1 and 2 versus morphing control bar actuation

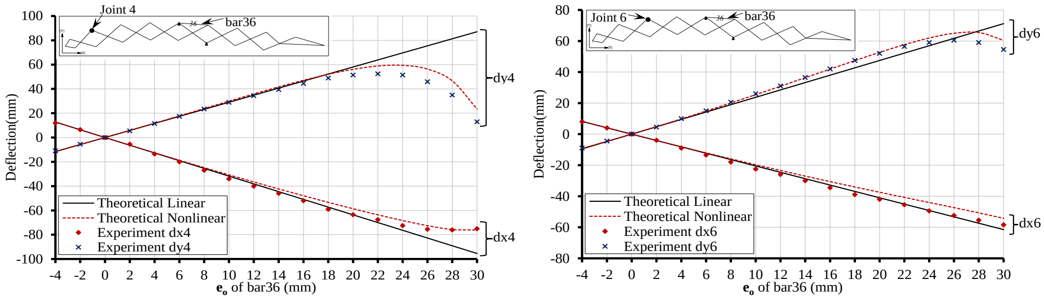

Fig. 8 Theoretical and experimental deflection of joints 4 and 6 versus morphing control bar actuation

geometric large geometric change in the structure through actuation in one or more morphing control bars. In the present experimental model, just one bar was selected for achieving the morphing process. Morphing is distinct to shape adjustment/controlling, since the adjustment process moves only small refinements in displacement and/or force changing, within essentially the same geometry, for the removing or reduction of any undesirable displacement and/or force, which can be carried out on either an unmorphable structure, or after morphing. The number of actuators for adjustment depends on the number of displacement or force variables.

As mentioned in the previous sections the structure of Fig. 5 is the demonstration of the morphing aerofoil structure. No doubt, many different shape configurations are necessary in any aircraft wing in order to achieve different lift and drag coefficients in the different stages of flight. In the experimental model, bar-36 was the morphing control bar, and the change in geometry achievable through actuation in bar 36 is shown in Fig. 6.

5.2 Calculation of morphing deflection

The comparison of experimental and analytical models is very important to prove the using of morphing structure for morphing aerofoil as an effective way to replace the tradition aerofoil. The deflection analysis is due to the loading and actuation of morphing control bar and can be calculated by Eq. (1). Furthermore, condensation in the force method was used for calculation where some of the displacements were “hidden” since they relate to unloaded joint components which were then condensed out from the primary equations. This is a novel approach and application.

Force method with matrix condensation technique was used for calculation of total displacement of the required joints, which contains two types of displacements. The first is the vector of nodal displacements of the structure due only to load, and the second is the resultant nodal displacements after some bar elongation actuation $\mathbf{e}_{oc}$ was applied. The combination of both deflections was done by superposition.

In this paper, an experiment has been done on a demonstration model of the morphing aerofoil shape structure as shown in Fig. 5 and compared to the theoretical results. In this experiment, one effective bar (bar 36) is selected to provide different shapes of the structure. Two methods for calculating theoretical nodal displacement of the pantographic morphing structure were introduced: linear and non-linear methods.

5.2.1 Linear calculation method

In the linear method nodal displacements of the structures were calculated through a single use of Eq. (1) in one iteration, with the same joint coordinates from the original shape of the model. Theoretical results of this method were compared with the experimental results as illustrated in Figs. 7 to 11, where the theoretically computed results were labelled as “Theoretical Linear” with solid lines. The results have a good correlation with the experimental results in the early stages of the structural shape morphing, typically until around $\mathbf{e}_o$=+10. Beyond that point, all the linear results begin to separate from the experimental trend line, except for *dx4*, *dx6* and *dy6* in Fig. 8 and *dx8* in Fig. 9 which continued in a straight line until approximately the end stages of the morphing. This separation is the result of non-linear behaviour of the structure for the morphing. Thus, the linear method is not

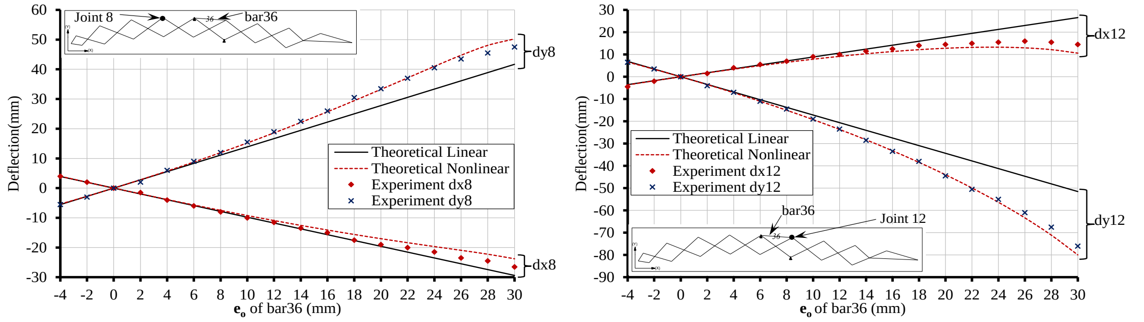

Fig. 9 Theoretical and experimental deflection of joints 8 and 12 versus morphing control bar actuation

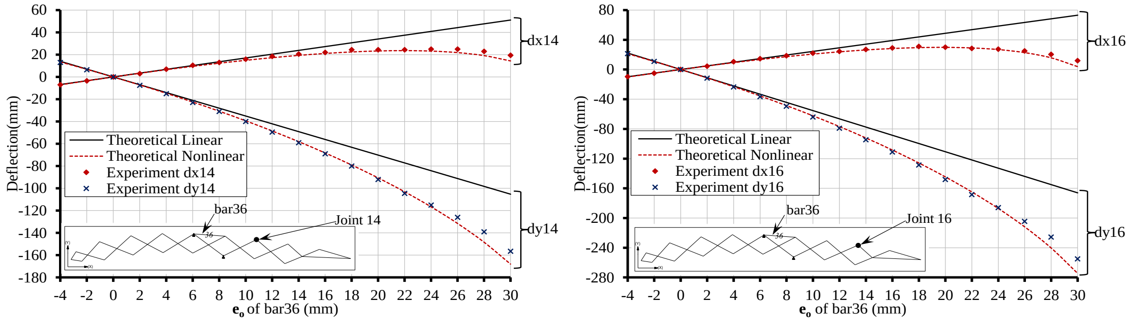

Fig. 10 Theoretical and experimental deflection of joints 14 and 16 versus morphing control bar actuation

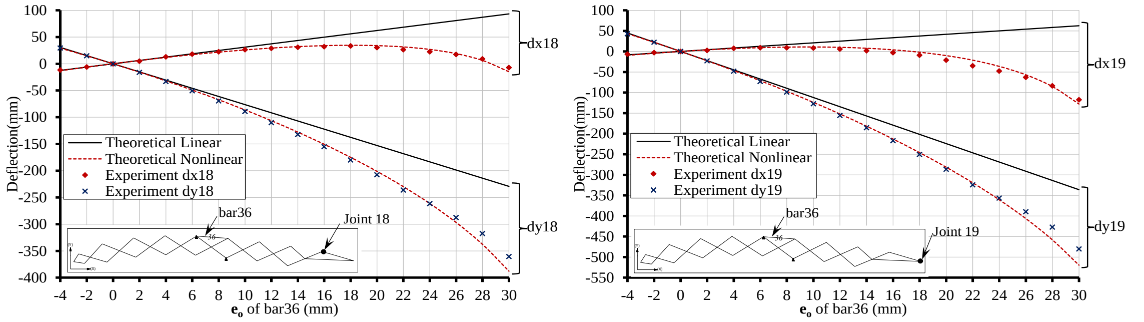

Fig. 11 Theoretical and experimental deflection of joints 18 and 19 versus morphing control bar actuation

valid for the full range of morphing and non-linear modification was proposed.

5.2.2 Non-linear calculation method (Coordinate Update Method)

Since the nonlinearity in the morphing structure was geometric, due to its flexibility and thus relatively large movements and displacements, the non-linear method for calculating the nodal displacements of the given model was based on updating the coordinate of the structure. In this method, Eq. (1) was used in the linear calculation method, within a number of cycles during which the coordinates of the structure were updated with the displacements in each iteration. The matrices of Equilibrium, Compatibility and Flexibility of the assembly are recalculated in each cycle although $\mathbf{F}^*$ changes only by a small amount due to very slight change in bar length from the changing coordinates. In other words, the calculation in each cycle is done for a "new" structure. The accuracy of the calculation increases with increasing the number of the iterations beyond the linear limit of displacement. Theoretical displacement results of this method have shown a very positive correspondence with the experimental measured displacement values (horizontal and vertical) of all joints as shown in Figs. 7 to 11.

In summary, as shown in Figs. 7 to 11, all the three curves correlate closely to each other at the early stages of morphing. Horizontal displacement results agree better with theoretical predictions than the vertical displacements in general. Some of the differences between non-linear and theoretical results could result from the shape of the physical model being imperfect from construction, and the imperfections exacerbate the distortion from theoretical shape at the later stages of morphing. However, as shown by the close correlation between the theoretical non-linear computation results and the experimental values, the main source of nonlinearity is geometric, and is due to the displacement prediction from a given structural geometry being no longer accurate or valid because that geometry had undergone significant change due to the morphing process. For sorting such kind of problems, the techniques for structure adjustment become necessary, as clarified in the next section.

6. Experimental and theoretical adjustment of imperfect shapes

In this paper, the focus has been on the behaviour of proposed morphing aerofoils. From the comparison of morphing results, only small differences were noticed between theoretical desired shapes and the measured experimental shapes of a physical model of the pantograph morphing aerofoil. Sometimes the model did not fit with the preferred shape due to structure loading, manufacture or assembly imperfection, or due to environmental effects (e.g., thermal distortion) or the structure moving. For this purpose, the technique of structure shape adjustment was applied to restore the shape to the desired shape. The necessary information is simply the displacements of the outside joint of the morphing aerofoil to be controlled (i.e., not all the displacements) as they stand, and what values they should become. Eq. (1) is the governing equation of this technique, and it specifically isolates the effects due to $\mathbf{e}_{oc}$ from any other effects.

An attempt was made to control displacements of joint linearly through finding a required set of actuations $\mathbf{e}_{oc}$ directly in one cycle of actuation. Then the adjustment was done theoretically and experimentally on the model, applying the calculated set of $\mathbf{e}_{oc}$ actuations to all selected bars to reach the target shape. Some experiments were done as shape adjustment on the model, after morphing other experiments were done for adjustment of the model with attached elastic bands between two adjacent external joints of the model, to simulate the effect of high strain stretchable skin on the surface of the aerofoil. Furthermore, experiments of multi-iteration adjustment were also done to reduce and remove errors arising from experimental work. Since this work is on the demonstration of the morphing aerofoil structure as an application of a morphing pantographic structure, the emphasis will be to control the shape of the structure, especially the upper surface, lower surface and the leading edge of the aerofoil, due to their role on the coefficients of lift and drag.

6.1 Adjustments for distributed vertical load

An aerofoil structure must be designed to withstand a large number of different types of loads and one of them is the aerodynamic load which is a distributed load as the result of pressures and shear stresses distributed over the aerofoil surface (Brandt *et al.* 2004). Therefore, the adjustment in this experiment was done under "distributed" vertical load at the joints. Vertical displacement control of the top surface of the structure in Fig. 5 is illustrated in Table 1. Actuation is applied in ten beams of the structure. After entering the target shape for the pre-adjustment displacement of the desired joints into Eq. (1), the amount of actuation of each member with an actuator already embedded was calculated.

Generally, the number of bars selected for actuation was sufficient, i.e., the possibility of achieving desired displacement target could be guaranteed in this structure. All the selected bar elongations were among non-vanishing components in the condensation process. The structure was thus adjusted practically in the laboratory according to the set of actuations.

Values of various parameters for the measured structure are shown in Columns 1 to 4 of Table 1. For the purpose of examining the efficiency of adjustment, it is presumed that the desired displacements are those shown in Column 6 of Table 1, which represent a more smooth top surface shape. This set of desired displacements represents significant deviation from the existing measured displacements in Column 4 and hence it is a reasonably good test of adjustment of a distorted model. The computed set of $\mathbf{e}_{oc}$ is shown in Column 5 of Table 1. Post-adjustment vertical displacement results (Column 7) are in good agreement with the target position (Column 6) as also shown in Fig. 12, with only small deviations. The source of this deviation is the combination of errors from imperfection in the geometrical construction of the structure and measurement of its coordinates, and additional flexibility in the structure due to turnbuckles with some slack in the bars. It is clear that the joints furthest from the support have more deviation than those closer. The total actuation in this experiment was 10.05 mm, through the same results could have been achieved with less actuation by selecting the most effective bars for these displacements, see Section 6.7 later on, which gives minimum actuation for controlling vertical displacement of the upper surface for any loading and any target position. For this set of actuators which have not been optimally chosen according to any objective, some of the selected bars would likely be working to some extent against each other.

6.2 Adjustments for distributed vertical load after morphing

In this experiment, the structure is tested under the same loading case as in Section 6.1 and also the same joint displacements are desired to be controlled, with the different starting shape of the structure since the structure is tested after shape morphing. The morphing is the result of lengthening the control bar by +10mm and the structure increases in both overall length and curvature. The new shape (in nodal coordinates) and different nodal displacements under load (Column 4) in Table 2, the target position of the of those joints required to be control are also consequently different as shown in Column 6 of Table 2.

The actuation $\mathbf{e}_{oc}$ for this experiment is calculated with Eq. (1), together with including the +10mm initial elongation to the morphing control bar (bar-36). The set of $\mathbf{e}_{oc}$ for this experiment is shown in Column 5 of Table 2, with the total actuation of 14.22 mm. Consequent to the adjustment, the measured displacements are as shown Column 7 of Table 2. Again, the difference between post-adjustment measurement and target position is small.

Table 1 Vertical displacement control of the upper surface joints of the structure in Fig. 5 under distributed

(1)	(2)	(3)	(4)	(5)	(6)	(7)	(8)
Joint	Dir.	P (N)	d_c (mm)	$\mathbf{e_{oc}}$ (mm)	d_{pc}, after $\mathbf{e_{oc}}$ (mm)		Bar
					Theo.	Prac.	
1	y	-2.286	-13.44	0.89	-9	-9.45	4
2	y	-2.286	-12.85	0.84	-8	-8.58	5
4	y	-2.286	-9.56	-1.72	-5	-5.11	12
6	y	-2.286	-5.44	-0.82	-3	-2.99	13
8	y	-2.286	-2.13	1.58	-1	-1.13	17
12	y	0	0.47	-0.24	0	0.13	20
14	y	-2.286	-0.41	1.60	0	0.23	24
16	y	-2.286	-2.14	-0.11	-1	-0.96	25
18	y	-2.286	-4.33	-0.79	-2	-2.13	28
19	y	-2.286	-7.31	-1.46	-3	-3.07	29
		total (mm)		10.05			

Table 2 Vertical displacement control of the upper surface joints of the morphed shape of the structure in Fig. 5 with (+10 mm) eoc of bar-36, under distributed vertical load

(1)	(2)	(3)	(4)	(5)	(6)	(7)	(8)
J	Dir.	P (N)	d_c (mm)	$\mathbf{e_{oc}}$ (mm)	d_{pc}, after $\mathbf{e_{oc}}$ (mm)		Bar
					Theo.	Prac.	
1	y	-2.286	20.73	-0.29	15	15.74	4
2	y	-2.286	19.12	2.51	15	15.36	5
4	y	-2.286	19.45	1.26	15	15.90	12
6	y	-2.286	18.30	0.17	15	15.04	13
8	y	-2.286	11.76	-1.32	10	9.84	17
12	y	0	-16.71	0.89	-15	-14.74	20
14	y	-2.286	-35.50	3.29	-30	-30.11	24
16	y	-2.286	-57.51	-1.07	-50	-50.55	25
18	y	-2.286	-80.76	1.72	-75	-75.93	28
19	y	-2.286	-119.36	-1.70	-110	-111.83	29
		total (mm)	14.22				

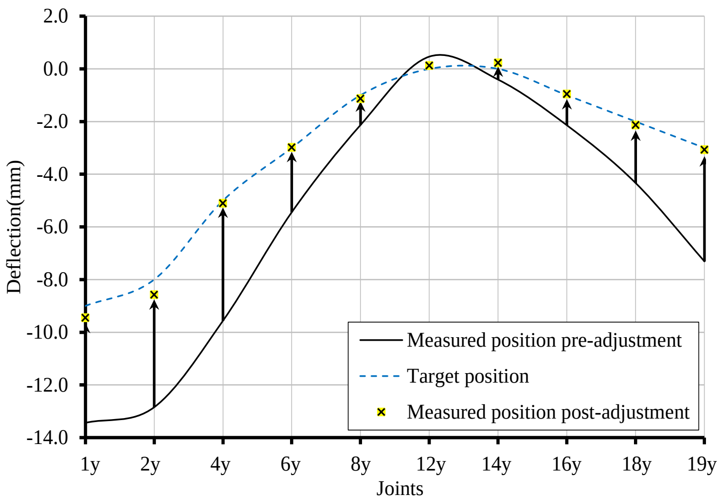

Fig. 12 Vertical displacement control of the upper surface joints of the structure in Fig. 5 under distributed vertical load

From this, it can be concluded that shape adjustment or refinement is likely to be possible for similar morphing structures for some specified joint displacements, with a fixed set of actuation members, in any stage of morphing. This is a positive result for the technology of designing morphing aerofoils, since not only have the static stages morphing aerofoil itself shown to have better aerodynamic characteristics than the equivalent fixed shape NACA aerofoil with flaps. Nonetheless here, we see that a morphing aerofoil which has gone "out of shape" due to changes in load or weight (e.g., through the burning of fuel normally stored within the voids of the aerofoil) can be corrected via shape adjustment. Furthermore, this leads to the possibility that a desired change in lift/drag characteristics could be obtained from either a morphing change or a smaller refining shape change, and thus the choice could be made dynamically during flight, and be optimised for best economy of flight operational parameters.

6.3 Adjustments for large vertical point load

In this section two experiments were done for two purposes, first to show that shape adjustment for a morphing structure is achievable for a concentrated load, and second to show that the choice of target position can have a large impact on the amount of total actuation in the adjustment process, through comparison results of these two experiments.

For the first purpose, the important point for designing an aerofoil is the very effectiveness in response and safety when unexpected forces act on the aerofoil, e.g., in storm conditions, as well as in more routine changes due to changing flight attitude, landing and take-off of an aircraft. While the aerofoil is expected to be subjected to distributed (and thus to a certain extent, even) loading when it is in service, sudden changes can cause a significant uneven loading that additionally twists the aerofoil. Therefore, a concentrated load was applied at the leading edge (frontal point) of the aerofoil to see how the adjustment techniques developed herein would help the distorted aerofoil to recover its shape and still meet design requirements of aerodynamic characteristics. In the given model as a demonstration of the aerofoil morphing structure, a single 10.287N load was vertically applied to joint 1 for both experiments. The pre-adjusted displacements are shown in Column 4 of Table 3. The same bars were chosen for actuation in both experiments with the different targets.

The new objective in these experiments is to control ten displacements through using only six bars for actuation. This case should thus be over-determinate and insoluble, and only a least-squares “approximate” is possible for e_{oc}. However in this particular structure, all five displacements chosen on the right hand side of the model (*12y*, *14y*, *16y*, *18y* and *19y*) (see Fig. 5 are affected by beam-pairs 19 and 20 and hence all these displacements can be controlled through actuation in bar 20 in this experiment. The other five displacements on the left hand side of the supports can be controlled by the other five actuators. Therefore, although the number of actuator is only six, there is still good control for the 10 joint displacements, as shown in Column 7 of Table 3. The results show good correlation with the desired displacements, which is restoring all displacement to the original pre-loading position with relatively only small deviations from the desired position.

The second purpose in this section is comparing the total required actuation for adjustment of the same structure (same loading, actuator position and number of actuators) with slightly different target positions for the selected joints for example the target *8y* displacement is -3mm, i.e., very close to the pre-adjustment displacement of -3.40mm instead of zero, while the amount of total actuation decreases from 13.96 mm to 5.06 mm, which is a significant amount. It shows that sometimes selecting targets for the experiment is challenging and needs high effort to control.

6.4 Adjustments for distributed horizontal load

In this section, an attempt was made to control horizontal displacements of the frontal joints of the structure of Fig. 5 against distributed horizontal loading which comes from the drag force of the wind during flying. The horizontal pre-adjustment displacements of the joints for control are shown in Column 4 of Table 4 due to the horizontal loading in Column 3. Through using only five actuators embedded to five beams, the aim of controlling those displacements was achieved. The amount of required actuation was calculated and shown in Column 5 with a total actuation of 7.04mm. Fig. 5 shows the post-adjustment displacements of the chosen joints relative $\mathbf{e}_{oc}$ the target position since the number of actuators is adequate for achieving the goal to secure this structure against horizontal loading.

6.5 Adjustments for vertical distribute loading with elastic band

The pantographic morphing structure model is of a demonstration morphing of aerofoil, hence a “stretchable skin” is also necessary to provide an external surface that can ensure correct aerodynamic properties (Du and Ang 2012). In this section, 15 elastic bands were stretched between each two adjacent external top and bottom joints of structure, as shown in Fig. 13. The axial stiffness of the elastic bands (EA) is 10N. Approximately, an even prestress level of 2N is achieved in all elastic bands by using the algorithm suggested by Kwan and Pellegrino (1993) via shortening the length of each elastic rubber band by 20.5%. The prestressing of the structure removed any joint slack and also reduced geometric flexibility of the structure.

The structure was tested for adjustment of vertical displacement of the upper joints under vertical distributed load as shown in Column 3 in Table 5. The measured positions of the joints and the target position were introduced to Eq. (1) from which a set of actuations (Column 5) was obtained to adjust the pre-adjustment displacement in Column 3. All the chosen bars for actuation are the most effective bars (see Section 6.7 for this adjustment, except for bars 5 and 34 which were “second

Table 3 Vertical displacement control of the upper surface joints of the structure in Fig. 5 under big vertical point load

(1)	(2)	(3)	(4)	(5)	(6)	(7)	(8)	(9)	(10)	(11)
J	Dir.	P (N)	d_c (mm)	First target position			Second target position			Bar
				$\mathbf{e}_{oc}$ (mm)	displacement after $\mathbf{e}_{oc}$ (m		$\mathbf{e}_{oc}$ (mm)	displacement after $\mathbf{e}_{oc}$ (m		
					Theo.	Prac.		Theo.	Prac.	
1	y	-10.287	-21.54	-0.153	0.00	1.36	-0.197	0.00	2.75	4
2	y	0	-20.55	-0.442	0.00	1.39	0.089	0.00	2.76	5
4	y	0	-15.19	-5.820	0.00	1.23	-3.314	0.00	2.03	12
6	y	0	-8.59	-1.975	0.00	0.97	-0.109	0.00	1.17	13
8	y	0	-3.40	4.917	0.00	0.24	-0.699	-3	-2.45	17
12	y	0	1.25	-0.650	0.00	0.13	-0.650	0.00	-0.11	20
14	y	0	1.39		0.00	0.05		0.00	0.06	
16	y	0	1.71		0.00	-0.05		0.00	-0.06	
18	y	0	2.10		0.00	0.36		0.00	-0.11	
19	y	0	3.60		0.00	0.11		0.00	0.07	
		total (mm)		13.96			5.06			

Table 4 Horizontal displacement control of the front joints of the structure Fig. 5 against distributed horizontal load

(1)	(2)	(3)	(4)	(5)	(6)	(7)	(8)
J	Dir.	P (N)	d_c (mm)	$\mathbf{e}_{oc}$ (mm)	d_{pc}, after $\mathbf{e}_{oc}$ (mm)		Bar
					Theo.	Prac.	
1	x	2.286	4.24	-1.27	1	1.98	4
2	x	2.286	4.00	1.06	0	0.78	5
4	x	2.286	2.99	2.25	0	0.41	12
6	x	2.286	1.72	-1.68	0	0.22	13
8	x	2.286	0.65	0.39	0	0.13	17
				-0.38			20
		total (mm)		7.04			

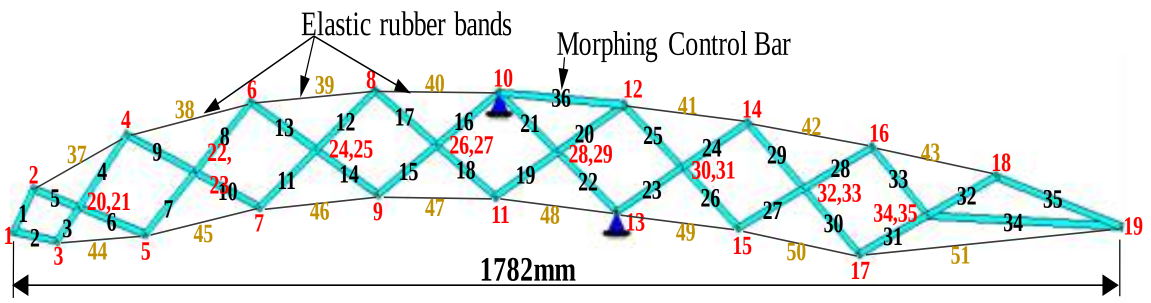

Fig. 13 Structure in Fig. 5 after increasing elastic rubber bands

best" options but nonetheless chosen instead of the best bars 1 and 35 because these two bars did not actually have an actuator. Consequently, the total actuation was 4.34 mm which was relatively very small. The numerical results are shown in Column 7, which shows the adjustment process is capable of countering the displacement due to the prestress and loading.

This experiment shows that using an elastic stretchable material is a suitable technique for the pantographic morphing structure skin to ensure correct aerodynamic properties of the aerofoil. In addition, it was also shown that the direct method of controlling displacement is valid and practical, and good for adjusting static shape induced by both loads (routine and unpredicted) and other factors such

Table 5 Vertical displacement control of the upper surface joints of the structure in Fig. 5 with elastic rubber bands

(1)	(2)	(3)	(4)	(5)	(6)	(7)	(8)
J	Dir.	P (N)	d_c (mm)	$\mathbf{e_{oc}}$ (mm)	d_{pc}, after $\mathbf{e_{oc}}$ (mm) Theo.	Prac.	Bar
1	y	-2.286	-13.672	-0.237	-1	-2.439	4
2	y	-2.286	-12.976	-0.226	-1	-1.823	5
4	y	-2.286	-9.829	-0.513	-1	-1.058	8
6	y	-2.286	-5.838	-1.152	-1	-1.227	12
8	y	-2.286	-2.395	-0.495	-1	-1.001	16
12	y	0	0.700	-0.364	0	0.285	20
14	y	-2.286	0.020	-0.378	0	0.762	25
16	y	-2.286	-1.501	-0.068	-1	-0.489	29
18	y	-2.286	-3.501	-0.743	-1	-0.169	33
19	y	-2.286	-5.640	0.171	-1	0.508	34
		total (mm)		4.34			

Table 6 Double iteration displacement control of the structure in Fig. 13

(1)	(2)	(3)	(4)	(5)	(6)	(7)	(8)	(9)	(10)
J	Dir.	P (N)	Iteration (1) d_c (mm)	$\mathbf{e_{oc1}}$ (mm)	displacement after Theo.	Prac.	Iteration (2) $\mathbf{e_{oc2}}$ (mm)	displacement after Prac.	Bar
1	y	-2.286	-13.672	-0.203	0	-0.293	-0.327	0.035	4
2	y	-2.286	-12.976	-0.215	0	0.208	-0.771	0.111	5
4	y	-2.286	-9.829	-0.396	0	0.379	0.003	-0.123	8
6	y	-2.286	-5.838	-0.757	0	0.127	0.160	0.107	12
8	y	-2.286	-2.395	-1.009	0	-0.121	0.029	-0.111	16
12	y	0	0.700	-0.363	0	0.290	-0.151	-0.103	20
14	y	-2.286	0.020	-0.378	0	0.574	0.126	0.098	25
16	y	-2.286	-1.501	-0.542	0	0.948	0.055	-0.012	29
18	y	-2.286	-3.501	-0.402	0	0.424	0.425	-0.131	33
19	y	-2.286	-5.640	0.097	0	0.760	-0.108	-0.216	34
total (mm)				4.36			2.15		

as from prestressing in the pantographic structures via using elastic bands. The prestress level of the elastic bands was not much affected by the adjustment process since the prestress was produced by shortening of the order of 20% strain, which is many times greater than the strain change due to the adjustment process.

6.6 Multi-iteration adjustment to remove practical errors

The nodal position defines the shape of the structure, and in this paper so far the control of the nodal displacements to restore structural shape has been carried out by a single application of the length actuation. Sometimes a very high geometric accuracy is necessary in some structures. One of these is the proposed pantographic morphing structure as an aerospace structure, where its functions, and the efficiency with which it carries out those functions, are very sensitive to structural shape. At other times, the target shape may be quite different from the starting shape.

It may be too difficult to achieve the required high geometric accuracy through only one iteration of the adjustment process, and a second or more iteration is necessary to deal with residual errors remaining after the first round. For solving this issue, the process of multi-iteration adjustment was applied through using Eq. (1) in two or more iterations. In this technique, simply the post-adjustment displacement from the first iteration is re-introduced as a pre-adjustment displacement in the next iteration, and so on, until the best possible adjustment is achieved. Again, in this test, the external joint of the morphing aerofoil was been controlled.

Table 7 Bar sensitivity to the vertical and horizontal displacement of the upper surface joints of the structure in Fig. 5.

bar	$\mathbf{e}_{oc}$	A. Bar sensitivity to the vertical displacement										B. Bar sensitivity to the horizontal displacement									
		d_{1y}	d_{2y}	d_{4y}	d_{6y}	d_{8y}	d_{12y}	d_{14y}	d_{16y}	d_{18y}	d_{19y}	d_{1x}	d_{2x}	d_{4x}	d_{6x}	d_{8x}	d_{12x}	d_{14x}	d_{16x}	d_{18x}	d_{19x}
1	1	-1.08	0	0	0	0	0	0	0	0	0	-0.17	0	0	0	0	0	0	0	0	0
2	1	0.60	0	0	0	0	0	0	0	0	0	-0.92	0	0	0	0	0	0	0	0	0
3	1	0.33	0	0	0	0	0	0	0	0	0	-0.51	0	0	0	0	0	0	0	0	0
4	1	-1.98	-1.81	0	0	0	0	0	0	0	0	-0.25	-0.52	0	0	0	0	0	0	0	0
5	1	-0.32	0.28	0	0	0	0	0	0	0	0	-0.05	-0.96	0	0	0	0	0	0	0	0
6	1	1.37	1.08	0	0	0	0	0	0	0	0	-1.16	-0.73	0	0	0	0	0	0	0	0
7	1	1.32	1.13	0	0	0	0	0	0	0	0	-0.53	-0.23	0	0	0	0	0	0	0	0
8	1	-3.49	-3.30	-2.15	0	0	0	0	0	0	0	-0.37	-0.66	-0.84	0	0	0	0	0	0	0
9	1	-0.93	-0.65	0.36	0	0	0	0	0	0	0	0.24	-0.19	-0.93	0	0	0	0	0	0	0
10	1	2.56	2.31	1.33	0	0	0	0	0	0	0	-1.59	-1.2	-0.55	0	0	0	0	0	0	0
11	1	2.96	2.75	1.55	0	0	0	0	0	0	0	-0.53	-0.22	0.03	0	0	0	0	0	0	0
12	1	-5.14	-4.93	-3.67	-2.05	0	0	0	0	0	0	-0.57	-0.89	-1.12	-1.06	0	0	0	0	0	0
13	1	-1.89	-1.64	-0.76	0.46	0	0	0	0	0	0	0.73	0.36	-0.30	-0.89	0	0	0	0	0	0
14	1	3.75	3.51	2.62	1.38	0	0	0	0	0	0	-1.97	-1.6	-0.97	-0.41	0	0	0	0	0	0
15	1	4.70	4.48	3.19	1.53	0	0	0	0	0	0	-0.42	-0.08	0.21	0.20	0	0	0	0	0	0
16	1	-6.83	-6.60	-5.26	-3.52	-1.95	0	0	0	0	0	-0.9	-1.25	-1.52	-1.48	-1.23	0	0	0	0	0
17	1	-2.93	-2.70	-1.89	-0.76	0.53	0	0	0	0	0	1.18	0.83	0.19	-0.39	-0.85	0	0	0	0	0
18	1	4.89	4.66	3.84	2.69	1.41	0	0	0	0	0	-2.18	-1.83	-1.23	-0.69	-0.29	0	0	0	0	0
19	1	6.45	6.21	4.86	3.10	1.48	0	0	0	0	0	-0.12	0.25	0.55	0.55	0.34	0	0	0	0	0
20	1	-2.92	-2.74	-2.48	-2.03	-1.19	1.93	2.14	2.64	3.22	5.54	3.83	3.54	2.72	1.75	0.84	0.13	-1.04	-2.17	-3.29	-2.62
21	1	-3.76	-3.55	-3.05	-2.30	-1.27	0.44	0.48	0.60	0.73	1.25	3.04	2.73	2.02	1.26	0.58	0.03	-0.23	-0.49	-0.74	-0.59
22	1	3.71	3.51	3.01	2.27	1.25	-0.43	-0.48	-0.59	-0.72	-1.24	-3.00	-2.69	-1.99	-1.24	-0.58	-0.03	0.23	0.49	0.73	0.59
23	1	0	0	0	0	0	0	1.34	2.6	3.84	4.63	0	0	0	0	0	0	0.46	0.96	1.49	1.72
24	1	0	0	0	0	0	0	0.44	-0.86	-2.14	-2.92	0	0	0	0	0	0	0.9	0.37	-0.19	-0.42
25	1	0	0	0	0	0	0	-2.01	-3.49	-4.99	-6.98	0	0	0	0	0	0	0.97	1.10	1.18	0.61
26	1	0	0	0	0	0	0	0	1.5	3.03	5.01	0	0	0	0	0	0	0	-0.12	-0.18	0.39
27	1	0	0	0	0	0	0	0	1.34	2.66	3.52	0	0	0	0	0	0	0	0.51	1.06	1.30
28	1	0	0	0	0	0	0	0	0.40	-0.89	-1.71	0	0	0	0	0	0	0	0.92	0.36	0.13
29	1	0	0	0	0	0	0	0	-2.11	-3.6	-5.6	0	0	0	0	0	0	0	0.91	1.01	0.44
30	1	0	0	0	0	0	0	0	0	1.44	3.33	0	0	0	0	0	0	0	0	-0.08	0.47
31	1	0	0	0	0	0	0	0	0	1.31	2.16	0	0	0	0	0	0	0	0	0.55	0.79
32	1	0	0	0	0	0	0	0	0	0.38	-3.32	0	0	0	0	0	0	0	0	0.93	-0.14
33	1	0	0	0	0	0	0	0	0	-2.08	-3.97	0	0	0	0	0	0	0	0	0.85	0.30
34	1	0	0	0	0	0	0	0	0	0	4.06	0	0	0	0	0	0	0	0	0	1.17
35	1	0	0	0	0	0	0	0	0	0	-4.22	0	0	0	0	0	0	0	0	0	-0.17
36	1	3.42	3.20	2.90	2.37	1.39	-1.72	-3.51	-5.54	-7.64	-11.21	-4.48	-4.14	-3.18	-2.05	-0.98	0.88	1.70	2.44	3.11	2.08

Table 6 Column 7 illustrates the results of adjustment, which comes from modifying the measured position of joints through applying the set of $\mathbf{e}_{oc}$ obtained from Eq. (1) to the structural model in the first iteration. The rms of the error after the first adjustments is still 0.49mm. This result is good but it was supposed that extra accuracy was necessary in the chosen nodes. To reduce the errors even further, a second iteration was done, and the results are shown in Column 9, where the rms error is now reduced to 0.12 mm.

On the basis of this experiment, it could be concluded that the technique of multi-iteration adjustment was effective in eliminating errors that occur in the practical adjustment process itself. The only problem in this experiment is the degree of measurement precision possible was of the order of the error in the second adjustment and hence it was difficult to particularly quantify the degree of improvement possible in a second iteration. It can be recommended that a very accurate non-contact measurement system should be used for the displacement measurement involving multi-iteration adjustment.

6.7 Finding most effective bars through calculating bar sensitivity to displacement

All prior adjustment experiments in this paper were carried out on actuators which were already in place, and consequently the question of which bars could be actuated did not arise; only the amount of actuation for the actuators available had to be calculated. Alternatively, at the early design stage where the location of actuators is still undecided, it is very important to locate the actuators in the components of the structure so that they could be of most effective in controlling future displacements.

In this section, “bar sensitivity” technique was used to highlight the most effective bars to carry the actuators.

Table 7 shows the vertical displacement of the upper surface pins due to successive unit actuation of each of the bars of Fig. 5. The table is compiled by assigning a unit elongation to each bar in turn, and the consequent values of these displacements are recorded. For example, when a unit elongation is applied to bar 1, a -1.08 mm displacement in d_{1y} results, but no other monitored displacement changes. On the other hand, when a unit elongation is applied to bar 20, all the monitored displacements are changed. Therefore, the non-zero values in this table show which bars are capable of controlling a certain displacement, and the largest coefficient for a particular displacement shows which bar has the most effective control for that displacement, while a “zero” shows a given bar has no control over these displacements. The computation of this technique was done through a specially used program in such a way the adjustment process follows the prepared data of Table 7.

To explain the process, experiment in Section 6.1 was chosen to apply this technique. In which the set of the vertical displacements (-13.44, -12.85, -9.56, -5.44, -2.13, 0.47, -0.41, -2.14, -4.33, -7.13) for the upper surface joints was adjusted through actuation in a set of pre-selected actuators in bars. The attempt to control all selected displacements was successful through the set of actuations (0.89, 0.84, -1.72, -0.82, 1.58, -0.24, 1.6, -0.11, -0.79, -1.46). However, the total actuation was 10.05 mm, which was relatively big, which we will reduce using the bar sensitivity technique.

The program starts with the control of d_{12y}, because it is affected by the least number of actuators, which are bars 20, 21 and 22. Then from these three bars, the most effective for an actuator is bar 20 with a 1.93 “bar sensitivity” so in the first cycle d_{12y} is directly controlled via actuation in bar 20 with the actuation of -0.24 mm. The calculated set of displacements for the second cycle after applying the actuation of bar 20 is (-12.73, -12.19, -8.96, -4.95 -1.84 d_{12y}=0, -0.93 -2.78, -5.11, -8.65). The actuation of bar 20 has effect on all displacements as shown in Table 7, and the displacement of joints on the left hand-side of supports are relatively reduced while the displacements of these right had-side are increased.

In the second cycle, d_{14y} is chosen for controlling since, with only six bars (20, 21, 22, 23, 24, and 25) able to affect it, it is the displacement with the next least number of possible actuators. Bar 25 is highlighted as the most effective bar, since even though bar 20 has a larger “bar sensitivity”, bar 20 has already been highlighted for controlling d_{12y}. Furthermore, bars 21 and 22 cannot be used for controlling d_{14y} either, because they are grouped with bar 20 for d_{12y} and any actuation now in bars 21 and 22 would affect d_{12y}. Consequently, for d_{14y}, out of the six possible bars, only the bottom three can be used, and bar 25 is the most effective of these three, and is thus selected. Together with the actuation in bar 20 for d_{12y}, the calculations show d_{14y} is directly controlled via actuation in bar 25 of -0.46 mm. The set of displacements after the second cycle becomes (-12.73, -12.19, -8.96, -4.96 -1.84, d_{12y}=0, d_{14y}=0, -1.17, -2.82, -5.44).

In the same way, d_{8y} is controlled in cycle three via -0.43 mm actuation in bar 16 and the displacements then become (-9.78, -9.33, -6.69, -3.43, d_{8y}=-1, d_{12y}=0, d_{14y} =0, -1.17, -2.82, -5.44). In the fourth cycle d_{6y} is controlled with its most effective bar, bar 12, with a -2.05 bar sensitivity coefficient, and an actuation of 0.21 mm the results of displacements are (-8.71, -8.30, -5.90, d_{6y}=-3, d_{8y}=-1, d_{12y}=0, d_{14y}=0, -1.17, -2.82, -5.44). The technique as described so far thus will continue until all displacements have achieved their targets. In this example, the program needed ten cycles to choose ten actuators for the 10 displacements to control. The whole set of actuation is (0.53, 0.62, -0.43, -0.21, -0.43, -0.24, -0.46, -0.08, -0.25, -0.23) with total actuation of 3.48 mm, while the total actuation in experiment in Section 6.1 with the same target displacements, but non-optimised actuator location) was of 10.05 m. The difference is significantly large, the use of the “bar sensitivity” technique has reduced the amount of actuation to around a third.

For highlighting the most effective bars for controlling horizontal displacements of joints in Fig. 5. Table 7 was prepared which illustrates coefficients of bar sensitivity to the horizontal displacements of the upper surface joints of the model. In a process similar to that for vertical displacements, it was shown that the most effective for effective bars for controlling (d_{1x}, d_{2x}, d_{4x}, d_{6x}, d_{8x}, d_{12x}, d_{14x}, d_{16x}, d_{18x}, d_{19x}) are bars (2, 5, 9, 12, 16, 20, 25, 28, 32, 35). Through using bar sensitivity technique the decision of where the actuator should be place can be taken before the designing of the structures. The advantages of this technique are both the minimum number of actuators as well as minimum actuation can be obtained, resulting in less expense and probably easier provision for control of structures.

7. Conclusions

The useful and relatively simple method has been applied in this paper, which provides a direct method for calculating required morphing shape displacements via finding most effective bar through calculating bar sensitivity to displacement. In addition, providing a direct relationship between bar length actuations and the nodal position/displacements for adjusting shape imperfection of the desired aerofoil theoretically and experimentally. The technique has been verified by experiments on the physical model of an aerofoil shaped morphing pantographic structure. So, the concept for a novel morphing aerofoil by pantographic morphing structure as an effective way to enhance/replace the tradition aerofoil has been proven.

Shape adjustment or refinement also can be done for any morphing structure for some specified joint displacements, with a fixed set of actuation members, in any stage of morphing. This is a good result for the technology of designing morphing aerofoils, since not only have the static stages morphing aerofoil itself shown to have better aerodynamic characteristics than the equivalent fixed shape NACA aerofoil with flaps, but here, we see that a morphing aerofoil which has gone "out of shape" due to changes in load or weight (e.g., through the burning of fuel normally stored within the voids of the aerofoil) can be corrected via shape adjustment.

Moreover, using an elastic stretchable material was found to be a suitable technique for the pantographic morphing structure skin to ensure correct aerodynamic properties of the aerofoil. In addition, it was also shown that the direct method of controlling displacement is valid and practical, and good for adjusting static shape induced by both loads (routine and unpredicted) and other factors such as from prestressing in the pantographic structures via using elastic bands. Furthermore, the technique of multi-iteration adjustment was presented that effective in eliminating errors that occur in the practical adjustment process itself, as demonstrated by the experiments on the physical model. Finally, the study discusses identification of the most effective bars with objective of minimal number of actuators or minimum actuation.

References

Akgün, Y. (2010), *A novel transformation model for deployable scissor-hinge structures*, PhD Thesis, Izmır Institute of Technology.

Alegria Mira, L. (2010), *Design and analysis of a universal scissor component for mobile architectural applications*, MSc Dissertation, Vrije Universiteit Brussel.

Bettini, P., Airoldi, A., Sala, G., Landro, L.D., Ruzzene, M. and Spadoni, A. (2010), "Composite chiral structures for morphing airofoils: Numerical analyses and development of a manufacturing process", *Compos. Part B: Eng*., **41**(2), 133-147. https://doi.org/10.1016/j.compositesb.2009.10.005.

Bliss, T.K. and Bart-Smith, H. (2005), "Morphing structures technology and its application to flight control", *Proceedings of the Student Research Conference*), Virginia Space Grant Consortium Newport News, Virginia, USA.

Brandt, S.A., Stiles, R.J., Bertin, J.J. and Whitford, R. (2004), *Introduction to Aeronautics: A Design Perspective*, 2nd edn. Reston, Virginia, USA, AIAA Education Series.

Chikahiro, Y., Ario, I., Nakazawa, M., Ono, S., Holnicki-Szulc, J., Pawlowski, P. and Graczykowski, C. (2014), "An experimental study on the design method of a real-sized Mobile Bridge for a moving vehicle", *Proceedings of the Mobile and Rapidly Assembled Structures IV*. (Eds., De Temmerman, N., and Brebbia, C.A.), WIT Press, Ostend, Belgium.

De Temmerman, N. (2007), *Design and analysis of deployable bar structures for mobile architectural applications*, PhD Thesis, Vrije Universiteit Brussel.

Du, S. and Ang, H. (2012), "Design and feasibility analyses of morphing airofoil used to control flight attitude", *J. Mech. Eng.*, **58**(1), 46-55.

Escrig, F. (1985), "Expandable space structures", *Space Struct. J.*, **1**(2), 79-91. https://doi.org/10.1177/026635118500100203.

Gantes, C.J. (2001), *Deployable Structures: Analysis and Design.* Southampton, UK, WIT Press.

Haftka, R.T. and Adelman, H.M. (1985a), "An analytical investigation of shape control of large space structures by applied temperatures", *AIAA J*., **23**(3), 450-457. https://doi.org/10.2514/3.8934.

Haftka, R.T. and Adelman, H.M. (1985b), "Selection of actuator locations for static shape control of large space structures by heuristic integer programing", *Comput. Struct.*, **20**(1-3), 575-582. https://doi.org/10.1016/0045-7949(85)90105-1.

Hoberman, C. (1990), Reversibly expandable doubly-curved truss structure), United States Patent no. 4, 942, 700.

Iannucci, L. and Fontanazza, A. (2008), "Design of morphing wing structures", *Proceedings of the 3rd Systems Engineering for Autonomous Systems (SEAS) Defence Technology Centre (DTC) Technical Conference*), Edinburgh, UK.

Inoue, F. (2007), "Development of adaptive construction structure by variable geometry truss", *Proceedings of the International Symposium Shell and Spatial Structures-Architectural Engineering-Towards the future looking to the past*. (Eds., Balaguer, C., and Abderrahim, M.), Venice, Italy.

Jensen, F. and Pellegrino, S. (2005), "Expandable 'blob'structures",. *J. Int. Association for Shell and Spatial Struct*., **46**(149), 151-158. https://doi.org/10.1142/9789812837219_0013.

Kwan, A.S.K. and Pellegrino, S. (1993), "Prestressing a space structure", *AIAA J*., **31**(10), 1961-1963. https://doi.org/10.2514/3.11876.

Lachenal, X., Weaver, P.M. and Daynes, S. (2012), "Multi-stable composite twisting structure for morphing applications", In *Proceedings of the Royal Society A: Mathematical, Physical and Engineering Science*), vol. 468, 1230-1251.

Maden, F., Korkmaz, K. and Akgün, Y. (2011), "A review of planar scissor structural mechanisms: geometric principles and design methods", *Architect. Sci. Review*, **54**(3), 246-257. https://doi.org/10.1080/00038628.2011.590054.

Merchan, C.H.H. (1987), *Deployable structures*, MSc Dissertation, Massachusetts Institute of Technology, Department of Architecture.

Pinero, E.P. (1961), "A reticular movable theatre", *The Architects' J.*, **134**, 299.

Roovers, K. and De Temmerman, N. (2014), "The design of a foldable triangulated scissor grid for single-curvature surfaces. *Proceedings of the Mobile and Rapidly Assembled Structures IV*. (Eds., De Temmerman, N. and Brebbia, C.A.), WIT Press, Ostend, Belgium.

Saeed, N.M. (2014), *Prestress and deformation control in flexible structures*, PhD Thesis, Cardiff University, Cardiff, UK.

Saeed, N.M. and Kwan, A.S.K. (2014), "Concepts for morphing aerofoil sections using pantographic structures", *Mobile and Rapidly Assembled Structures IV*, **136**, 279.

Saeed, N.M. and Kwan, A.S.K. (2016), "Displacement and force control of complex element structures by Matrix Condensation", *Struct. Eng. Mech*., **59**(6), 973-992. http://dx.doi.org/10.12989/sem.2016.59.6.973.

Subramanian, G. and Mohan, P. (1996), "A fast algorithm for the static shape control of flexible structures", *Comput. Struct*., **59**(3), 485-488. https://doi.org/10.1016/0045-7949(96)00266-0.

Wolfe, M.H. (2013), *Analysis of deployable strut roof structures*, MSc Dissertation, Massachusetts Institute of Technology.

You, Z. (1997), "Displacement control of prestressed structures", *Comput. Method. Appl. M*., **144**(1-2), 51-59. https://doi.org/10.1016/S0045-7825(96)01164-4.

You, Z. and Pellegrino, S. (1997), "Foldable bar structures", *Int. J. Solids Struct*., **34**(15), 1825-1847. https://doi.org/10.1016/S0020-7683(96)00125-4.

HJ